

Spatiotemporal Dynamics of the BOLD fMRI Signals: Toward Mapping Submillimeter Cortical Columns Using the Early Negative Response

Timothy Q. Duong, Dae-Shik Kim, Kâmil Uğurbil, and Seong-Gi Kim*

The existence of the early-negative blood-oxygenation-level-dependent (BOLD) response is controversial and its practical utility for mapping brain functions with columnar spatial specificity remains questionable. To address these issues, gradient-echo BOLD fMRI studies were performed at 4.7 T and 9.4 T using the well-established orientation column model in the cat visual cortex. A robust transient early-negative BOLD response was consistently observed in anesthetized cat ($-0.35 \pm 0.09\%$, mean \pm SD, $n = 8$ at 2.9 ± 0.5 sec poststimulus onset for 4.7 T, TE = 31 ms; $-0.29 \pm 0.10\%$, $n = 4$ at 3.0 ± 0.8 sec poststimulus onset for 9.4 T, TE = 12 ms). In addition to its temporal evolution, the BOLD response also evolved dynamically in the spatial domain. The initially spatially localized early-negative signal appeared to dynamically drain from the active sites toward large vessels, followed by a wave of the delayed positive signal, which exhibited similar spatiotemporal dynamics. Only the early-negative BOLD response within 2 sec of the stimulus onset (not the entire dip) yielded columnar layouts without differential subtraction. The functional maps of two orthogonal orientations using the first 2-sec dip were indeed complementary. On the other hand, the delayed positive BOLD response appeared diffused and extended beyond the active sites. It was thus less suitable to resolve columnar layouts. These results have implications for the design and interpretation of the BOLD fMRI at columnar resolution. Magn Reson Med 44:231–242, 2000. © 2000 Wiley-Liss, Inc.

Key words: early dip; brain mapping; deoxyhemoglobin; oxygen consumption; cerebral blood flow; ocular dominance columns; high magnetic field; cat visual cortex; optical imaging; orientation columns; hemodynamic response

Blood oxygenation level dependent (BOLD) functional MRI (fMRI) (1) has been extensively used to noninvasively map human brain processes (2–4), ranging from sensory perception to cognitive function. The stimulus-induced BOLD contrast arises from regional changes in paramagnetic deoxyhemoglobin concentration and, thus, can be detected in $^1\text{H}_2\text{O}$ T_2^* -weighted images (1). Despite the indispensable role of the BOLD fMRI technique in mapping human brain functions (typically on the coarse scale of a few millimeters), the source of the BOLD signal in relation to the site of neuronal activity remains poorly understood and controversial (5,6). Further, it is unclear whether the conventional BOLD response has sufficient spatial speci-

ficity to map submillimeter functional structures (e.g., cortical columns) (7,8).

At the heart of this spatial limitation is the hemodynamic response per se. Recent optical spectroscopy studies of orientation columns in the cat visual cortex suggested that the delayed hemodynamic response of the oxyhemoglobin increase is diffused and extends far beyond the true activated site, resulting in a fundamental spatial limitation of 2–3 mm resolution (9,10). Based on such findings, it was concluded that signals from the delayed oxyhemoglobin increase are insufficient to resolve functionally active, individual orientation columns (~ 500 μm in diameter) that are ~ 1.3 mm apart (11). On the other hand, the initial “metabolism-based” deoxyhemoglobin signal increase was reported to be spatially confined to the site of increased neuronal activity. “Patchy” orientation column layouts, consistent with the 2-deoxyglucose (2-DG) autoradiographic data (11) and single-unit recording (12), were resolved by using this transient deoxyhemoglobin signal increase (9). These results have strong implications for the BOLD fMRI technique, which is based on similar hemodynamic and metabolic principles for detection of neuronal activity. Essentially all BOLD studies aimed at mapping brain function to date employ the delayed positive BOLD response, corresponding to the delayed increase in the optical oxyhemoglobin signals. Therefore, in principle the conventional BOLD technique also suffers from a fundamental limitation in spatial resolution of similar magnitude. Engel et al. (7) and Menon and Goodyear (8) recently demonstrated that this is indeed the case.

Interestingly, mapping ocular dominance columns in human using the delayed positive BOLD response has been attempted by using the “differential imaging” method in which functional maps were generated by subtracting the BOLD signals of two complementary stimuli (i.e., left and right eye visual stimuli) (8,13). While the use of the differential subtraction method in optical imaging studies has been well established via extensive verifications with the single-unit (12) and 2-DG (11) technique, the validity and implications of this method on the BOLD fMRI data at columnar resolution, however, remain unresolved and poorly understood. Further, this subtraction approach can only be used with the assumption that the activation areas are complementary (i.e., exact knowledge of the hypothesis under test). Consequently, this method cannot be readily used to map most cerebral functions, as the majority of the functional units in the brain are not complementary. It is thus desirable to obtain columnar structures using a single-stimulus condition (“single-condition” map) without using the differential imaging method.

Center for Magnetic Resonance Research, Department of Radiology, University of Minnesota School of Medicine, Minneapolis, Minnesota.

Grant sponsor: NIH; Grant numbers: RR08079; NS38195; MH60724; NS10930; Grant sponsors: Keck Foundation; Minnesota Medical Foundation.

*Correspondence to: Seong-Gi Kim, Ph.D., Center for Magnetic Resonance Research, University of Minnesota School of Medicine, Radiology, 2021 Sixth Street SE, Minneapolis, MN 55455. E-mail: kim@cmrr.umn.edu

Received 16 November 1999; revised 6 March 2000; accepted 13 April 2000.

Prompted by the optical spectroscopy data that the initial deoxyhemoglobin increase following increased neuronal activity is spatially more localized than the subsequent oxyhemoglobin increase, several fMRI studies have been carried out to search for the initial increase in regional deoxyhemoglobin, which is expected to give rise to an early negative BOLD response (“dip”). To date, the existence of the early negative BOLD response remains debated. A small, transient negative BOLD response has been detected in the human visual cortex (14–19) and, very recently, in the monkey visual cortex (20). On the other hand, Jezard et al. (21) reported no early negative BOLD response in the cat visual cortex. Similarly, the dip was not observed in the rat somatosensory cortex (22,23). These discrepancies regarding the existence of the dip remain largely unexplained and raise the question of whether the early negative BOLD signal has the same biophysical basis as the intrinsic deoxyhemoglobin optical signal. Furthermore, the practical significance of the initial negative BOLD response, namely, whether it can be used to noninvasively map brain functions with *columnar resolution*, remains elusive. This is because of the small amplitude (percent change) of the dip in combination with the need to achieve high spatial and temporal resolution for columnar mapping.

Herein, we present a BOLD fMRI study using the well-established orientation-column model in cat in which the initial increase in the stimulus-induced deoxyhemoglobin signal was originally observed using the optical spectroscopy technique (9,24). The aims of this study were to use this cat model to: 1) determine whether an early-negative fMRI BOLD response can be robustly detected; 2) evaluate the spatial specificity of different temporal phases of the BOLD response; and 3) examine their ability to map brain functions at columnar resolution (i.e., to resolve functionally activated structures of $\sim 500\ \mu\text{m}$ in size that are $\sim 1.3\ \text{mm}$ apart) by using a “single-stimulus” condition. High spatiotemporal resolution BOLD measurements at high magnetic fields of 4.7 and 9.4 T were made. A robust transient early-negative BOLD response was observed, consistent with the interpretation that there was an initial increase in cerebral metabolic rate of oxygen (CMRO₂) following increased neuronal activity (25). Functional maps generated using the early-negative responses (only within 2 sec following the stimulus onset) were consistent with the layout of orientation columns and functional maps of orthogonal stimuli were highly complementary. Both the delayed negative BOLD (i.e., 2–4 sec poststimulus onset) and delayed positive BOLD responses, on the other hand, appeared diffused and less suitable to resolve columnar structures. The neuroscience application of this methodology has recently appeared in a companion article (26).

METHODS

Animal Preparations

All animal experiments were performed with institutional approval. A total of 12 independent studies were performed on 6 cats (fMRI was done more than twice in some animals, while only once in others). Female adolescent

cats (0.5–1.1 kg, 6–10 weeks old) were treated with atropine sulfate (0.05 mg/kg, i.m.) and anesthetized with a ketamine (10–25 mg/kg) and xylazine (2.5 mg/kg) cocktail (i.m.). The forepaw vein was catheterized for fluid supplement. The animal was orally intubated and mechanically ventilated using a Harvard ventilator ($\sim 35\text{--}45$ stroke/min, 15–30 ml/stroke) under isoflurane anesthesia (1.0–1.3% v/v) in a 1:1 N₂O:O₂ mixture throughout the experiment. End-tidal pCO₂ was continuously monitored using a capnometer (Datex-Ohmeda, Louisville, CO) and kept within normal physiological ranges (3–4%). The animal’s pupils were dilated with a drop of atropine sulfate solution (Steris Lab, Phoenix, AZ) and the animal’s eyes were refracted with corrective contact lenses (Danker Lab, Sarasota, FL). The animal was then placed in a cradle and restrained in normal postural position using a head-holder consisting of eye, ear, and mouth bars. The animal’s rectal temperature was maintained at $38 \pm 1^\circ\text{C}$ throughout the experiments. At the end of the 3–5-h MR study, the isoflurane anesthesia was discontinued and the animal was kept on the respirator until she could breath on her own. The animal was observed for 0.5–2.0 h before being returned to her littermates.

Stimulation Paradigm

The stimulation paradigm employed herein was essentially identical to that used in optical spectroscopy studies (9,24). The visual stimuli (presented to both eyes) consisted of high-contrast, *drifting* square-wave gratings (0.15 cycle/degree, 2 cycle/s) of four different orientations (0°, 45°, 90°, and/or 135°). *Stationary* gratings of identical spatial frequency and orientation were presented during the resting period. The stimulus parameters were optimized to activate orientation selective neurons in area 18 of the cat visual cortex (which is functionally homologous to the primary visual cortex, area V1, in human and monkey). The visual stimuli were projected onto a screen from the back of the magnet using a video projector (with 640 × 480 pixel resolution, Resonance Technology Co., Northridge, CA). The screen was positioned $\sim 15\ \text{cm}$ from the animal’s eyes, covering about 37° of the visual field. Visual stimulation and image acquisition were synchronized using a home-built TTL-I/O device.

MR Experiments

MR experiments were performed on a 4.7 T/40-cm (Oxford Magnet Technology, Oxford, UK) or a 9.4 T/31-cm (MagneX Scientific, Abingdon, UK) horizontal magnets. The former was equipped with a home-built 15 G/cm gradient of 300 μs risetime (ID = 11 cm) and the latter with a 30 G/cm gradient (11.0 cm ID, 300- μs risetime; MagneX Scientific). The two MR scanners were independently driven by two identical ^{Unity}INOVA consoles (Varian Inc., Palo Alto, CA). Protocols and parameters used at both magnetic fields were identical unless otherwise specified. After placing the animal in a cradle, a small, high-sensitivity surface coil of 1.2 cm (at 4.7 T) or 1.4 cm (at 9.4 T) diameter was placed on top of the cat brain. By using a small surface coil, the field-of-view (FOV = 2 × 2 cm² and data matrix = 64 × 64) was reduced without aliasing,

resulting in improved spatial resolution for a given data matrix. A single 2-mm horizontal slice, ~ 0.5 mm below the cortical surface, was chosen to target the columnar structure in area 18 with minimal superficial vessel contamination. Area 18 on the lateral gyrus is essentially flat and, thus, can be covered by a single imaging slice. The parameters at 4.7 T were: single-shot gradient-echo (GE) echo-planar images (EPI), TR = 0.5 sec, TE = 31 ms, spectral width = 100 kHz, and flip angle = 40° . The parameters at 9.4 T were: two-segment GE EPI, TR = 0.5 sec (0.25 sec each segment), TE = 12 ms, spectral width = 170 kHz, and flip angle = 30° . For each BOLD fMRI measurement, a total of 160 images were acquired: 60 images prestimulation, 20 images during stimulation, and 80 images poststimulation.

Data Analysis

The EPI images were zero-filled from a data matrix of 64×64 to 128×128 , yielding a nominal in-plane resolution of $156 \times 156 \mu\text{m}^2$ ($310 \times 310 \mu\text{m}^2$ before zero filling). Multiple BOLD measurements from each imaging session were averaged together before further analysis. Image data analysis employed Stimulate (27) and software codes written in PV-WAVE (Visual Numerics, Houston, TX).

The first 30 images (15 sec) were discarded because the signal intensities were not yet at equilibrium. For improved efficiency, calculations were not done for pixels with very poor SNR (i.e., pixels outside the brain). These pixels were distinguished based on the standard deviation (SD) maps, which were calculated using the baseline images from 0–15 sec *before* stimulus onset. Only pixels with intensity SD $< 1.5\%$ were used for subsequent calculation. Two types of activation maps were computed, namely: cross-correlation maps and representative 2-sec “time-binned” percent-change maps. First, cross-correlation (CC) activation maps were computed using the boxcar cross-correlation method (28) with the CC coefficient threshold set at 98% confidence level (corresponding to a CC value of 0.3 (29)). Second, the BOLD time course from 0–10 sec after the stimulus onset was divided (“time-binned”) into five segments to obtain representative detailed spatiotemporal information on the BOLD response. The 2-sec image segments were: early-negative segment (0.5–2.0 sec *after* the stimulus onset), late-negative segment (2.5–4.0 sec), early-positive segment (4.5–6.0 sec), late-positive segment (6.5–8.0 sec), and late-late-positive segment (8.5–10.0 sec). For each “time-binned” map, individual pixels displaying percent changes (both positive or negative) with at least 0.6–1.0 SD away from the baseline were taken to be statistically significant (at least 73–84% confidence level), except for the late-positive and late-late-positive segment, where the statistical threshold *for the positive percent change* was raised in proportion to the contrast-to-noise ratio (CNR) of the maximum positive to the minimum negative BOLD response. Since the percent-change amplitudes of the late- and late-late-positive responses were larger than those of the early-negative and early-positive responses, correspondingly raising the statistical thresholds was justified because the activation maps with the smaller percent changes (i.e., early-negative segment) would otherwise falsely yield improved spatial localization.

A minimal cluster size of four pixels was further used to construct all activation maps, resulting in an improved statistical significance of at least 80–94% confidence level (30). The computed activation maps were overlaid on anatomical images. All reported values were in mean \pm SD and all statistical tests employed Student’s paired *t*-test unless otherwise specified.

RESULTS

Extensive measures were taken to enhance the stability and reproducibility of the BOLD responses. The end-tidal CO_2 was found to be critical for obtaining a stable and consistent BOLD response. Optimal and robust BOLD response was elicited with the end-tidal CO_2 maintained at 3.5–3.8% (within the normal physiological range) and isoflurane level at 1.1–1.2%. Note that the anesthesia level used herein was generally higher than that ($< 0.9\%$) typically used in some optical imaging studies, presumably because of the gradient acoustic noise, which left the animal at a more conscious state. Notably, the BOLD response was markedly attenuated at 1.5% isoflurane and was essentially abolished at $> 1.8\%$ isoflurane.

In a typical fMRI study session, 5–10 fMRI measurements were made, essentially all of which yielded excellent/good early-negative responses. The SD of the signal fluctuation obtained from a 1-cm^2 ROI during the control/nonstimulated period was $0.10 \pm 0.05\%$ of the signal (in a single measurement without signal averaging). Figure 1a–c shows the anatomical images and the slice positions used for the fMRI studies. Figure 1d shows a representative cross-correlation activation map of the cat visual cortex following visual presentation of a single (0°) orientation. The fMRI image is an oblique view of area 18 of the primary visual cortex, tangential to the cortical surface. The stimulus evoked a BOLD response in area 18, consistent with those reported in the optical spectroscopy literature (9,24) and an fMRI study (21) in cat. These CC maps are highly reproducible under test and retest conditions acquired at least 3 h apart. The CC maps, however, were relatively uniform, without the characteristic “patchy” appearance of the columnar structures. Rather, the activity was heavily concentrated along large vessels, particularly the superior sagittal sinus, which are presumably distant from the active sites. In fact, the CC maps of four different orientations (0° , 45° , 90° , and 135°) in the same study session yielded roughly homogeneous spatial distributions that were hardly distinguishable from each other (data not shown), in agreement with an earlier finding (21). These observations are also consistent with the optical literature (9), which demonstrated that the delayed increase of oxyhemoglobin optical signal was less suitable for discriminating columnar layouts. The nominal in-plane resolution of $\sim 156 \times 156 \mu\text{m}^2$ ($\sim 310 \times 310 \mu\text{m}^2$ before zero filling) herein should have been sufficient to resolve the functionally activated, individual columns of $\sim 500 \times 500 \mu\text{m}^2$ that are ~ 1.3 mm apart.

Figure 2 displays three representative BOLD time-courses obtained from all the activated pixels of the CC maps (i.e., from Fig. 1) in three independent studies at 4.7 T (similar data quality was obtained at 9.4 T). The temporal evolution of the BOLD response was clearly bipha-

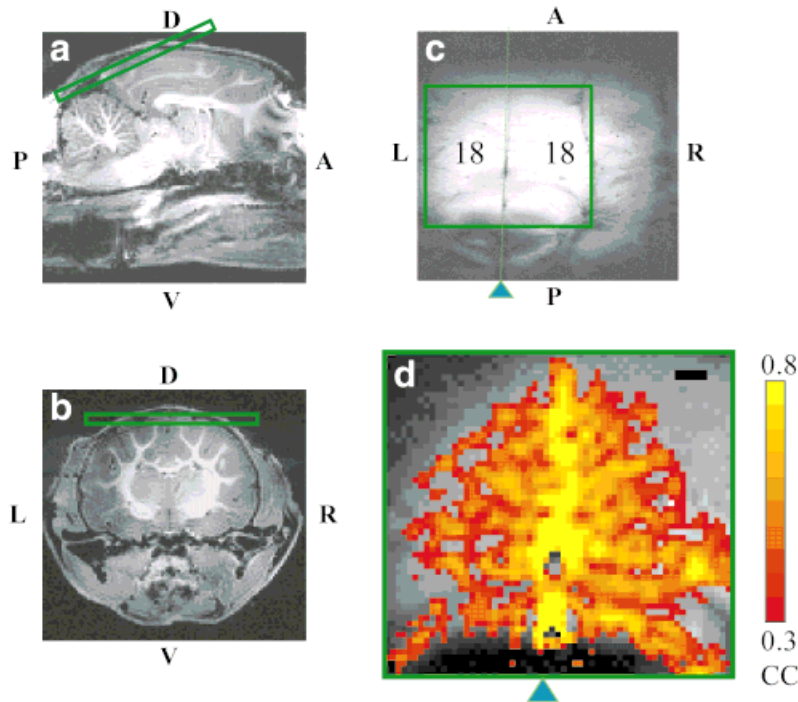


FIG. 1. Anatomical images and slice positions for the fMRI studies are shown in **a–c**. A representative cross-correlation (CC) map of the BOLD responses to a single orientation stimulus is shown in **d**. An expanded cross-correlation activation map of the BOLD response is overlaid on the anatomical image with the region of expansion shown in **c**, indicating area 18 of the visual cortex. A robust BOLD response in area 18 of the visual cortex was observed. Pixels with the highest statistical significance tended to align along the superior sagittal sinus. The signal of these activated pixels, however, were not of *intravascular* origin; rather, they arose from the bulk magnetic susceptibility effect around the sinus since the chosen slice lay ~ 0.5 mm inferior to the superficial vessels. The colored bar shows the scale of the cross-correlation coefficients. Scale bar in **d** is 1 mm. The arrowheads indicate the position of the midline. L, left hemisphere; R, right hemisphere; A, anterior; P, posterior; D, dorsal; and V, ventral. Note that the anatomical images in **a,b** were obtained with a volume coil using a 3D-MDEFT sequence (40) on a different animal. All BOLD studies and the anatomical image in **c** were obtained with a surface coil.

sic—an initial decrease, followed by a zero crossing and a delayed increase of the BOLD response is evident. The early-negative BOLD response shows a signal decrease of $\sim 0.4\%$ and reached its minimum ~ 3.0 sec after the stimulus onset. The conventional positive BOLD response shows a signal increase of $\sim 1.5\%$ and reached its maximum ~ 13 sec after the stimulus onset. The time to minimum of the early-negative BOLD and the time to maximum of the positive BOLD for each fMRI study at 4.7 T and

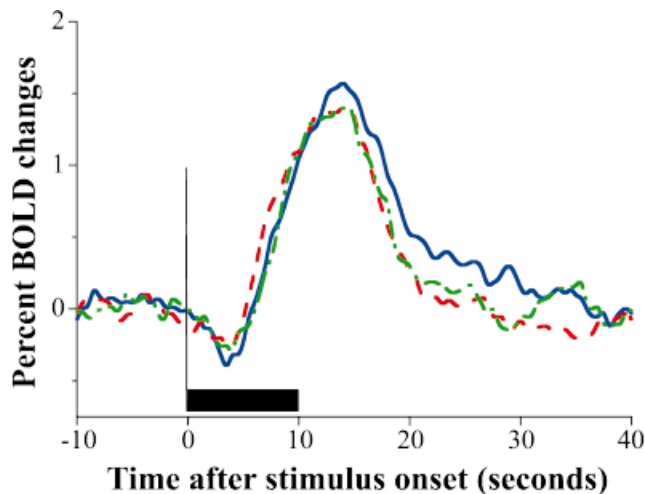


FIG. 2. Representative time-courses of the BOLD responses from the CC maps obtained from three independent studies. The time-courses were obtained with signal averaging of six (red dashed line), eight (green dotted line), and ten (blue solid line) measurements. The black rectangular block indicates the 10-sec stimulus duration. The temporal evolution of the BOLD response clearly showed a biphasic behavior—an initial decrease, followed by a zero crossing and a delayed increase of the BOLD response.

9.4 T are summarized in Table 1. These data are in good agreement with the optical imaging results in cat (9,24), BOLD fMRI results in humans (14–19), and a recent BOLD fMRI result in monkeys (20). Detailed quantitative cross-laboratory comparisons of the time-to-peak and percent changes of the negative BOLD responses and optical imaging data are summarized in Table 2.

In regard to the field dependence of the BOLD response, the time to minimum and time to maximum of the negative and positive BOLD responses and their percent changes were consistent between the two magnetic fields ($P > 0.2$). The ratios of the negative to the positive BOLD magnitudes were essentially identical (0.23 at 4.7 T and 0.22 at 9.4 T), suggesting similar spatial specificity was achieved at the two magnetic fields. The SNR and CNR at 9.4 T were slightly lower than 4.7 T, likely due to the shorter repetition time per segment at 9.4T.

Spatiotemporal Characteristics of the BOLD Responses

As a first step to characterize the spatiotemporal dynamics of the BOLD response, 2-sec “time-binned” activation maps were generated (Fig. 3). In sharp contrast to the CC maps, the early-negative segment map showed predominantly patchy activation patterns (blue/purple pixels) in area 18 but not around the sinus (Fig. 3a). These patchy patterns appeared to be column-like based on column size and spacing. The average cluster size of the activated pixels was ~ 300 – 500 μm and the distance between neighboring pixel clusters was $\sim 1.3 \pm 0.2$ mm, consistent with the dimensions of orientation columns visualized with the 2-DG technique (~ 500 μm and ~ 1.2 – 1.4 mm, respectively (11)). The clustered pixels are irregularly shaped, also consistent with those observed using the 2-DG (11,31) and optical imaging (32) methods. The late-negative segment map shows that the active (blue/purple) areas have moved

Table 1A
Percent Changes and Time-to-Peak of the Early-Negative and Delayed Positive BOLD Responses at 4.7 T (n = 8)^a

Study ^b	Time to min ^c	Time to max ^c	Min % change	Max % change
1	2.0	10.0	-0.40	1.4
2	2.5	10.0	-0.38	1.4
3	3.0	12.0	-0.43	1.6
4	3.5	9.5	-0.28	1.1
5	3.0	8.0	-0.20	1.1
6	2.5	6.0	-0.47	1.6
7	3.5	12.0	-0.30	1.1
8	3.0	8.5	-0.30	2.3
Mean ± SD	2.9 ± 0.5	9.5 ± 2.0	-0.35 ± 0.09	1.5 ± 0.4

^aData obtained from the CC maps with the minimum CC coefficient of ~ 0.3 , demonstrating that the early dip was observed across the entire the area 18 of the cat primary visual cortex. The CNR for the positive BOLD was 16 ± 5 (ranging from 11 to 18) at 4.7 T and ~ 10 for 9.4 T.

^bAt 4.7 T, study #1–5 were obtained from Cat #1, study #6–7 from Cat #2, and study #8 from Cat #3. At 9.4 T, study #1–2 were obtained from the same cat while study #3 and #4 were obtained from two different cats.

^cTime to min. or max. are the time (in sec) it took to reach the minimum or maximum.

toward the region of the sagittal sinus (Fig. 3b). This draining characteristic toward other large vessels was also observed in the time-frame movies (not shown) but was not as obvious as that toward the sagittal sinus. These observations suggest that the regional accumulations of deoxy-hemoglobin in active tissue were dynamically drained from capillaries into venules and veins. For consistency, pixels with positive percent changes during the first 4 sec after the stimulus onset were also computed. These pixels, shown as red/yellow in Fig. 3a,b, were most likely due to noise fluctuation and were not further analyzed.

As the late-negative response disappeared into the sinus, the early-positive response map started to show a patchy activation pattern in area 18 but not around the sinus (Fig. 3c, red/yellow pixels). The spatial dynamics of the positive response mimicked that of the negative response; namely, the patchy pattern appeared and subsequently disappeared as large positive changes became detectable in the draining sinus (Fig. 3c–e). However, the activated areas of the late- and late-late-positive segments were consistently and considerably larger than those of the negative segments. This is particularly apparent during the late-late-positive segment (Fig. 3e). Similarly, for consistency, pixels with negative percent changes during the 4–10 sec after the stimulus onset were computed. These pixels, shown as blue/purple in Fig. 3c–e, were most

likely due to noise fluctuation and were not further analyzed.

Note that even though the BOLD response lasted longer than 10 sec after stimulus onset, the BOLD responses beyond 10 sec after the stimulus onset were not presented here because the activation maps were very poorly localized (worse than that in Fig. 3e) and predominantly in large vessels. Similarly, activation maps generated by time-binning the poststimulus undershoot was not robust because the poststimulus onsets were highly variable and not consistently observed in all fMRI studies. Therefore, the BOLD responses beyond 10 sec after the stimulus onset were not further analyzed.

Complementary Test of Orthogonal Orientation Maps

Since the activation maps constructed by both the early-negative and early-positive segment showed patchy patterns consistent with columnar organization, further analysis was performed to evaluate their veracity. Activation maps were generated for two orthogonal orientation stimuli (i.e., 0° and 90° , or 45° and 135°). Based on the optical imaging (9,10) and single-unit recording (12) data, functional maps of two orthogonal orientations should be complementary. Figure 4a,b shows the combined maps of the two orthogonal orientations (45° and 135°) using the early-

Table 1B
Percent Changes and Time-to-Peak of the Early-Negative and Delayed Positive BOLD Responses at 9.4 T (n = 4)^a

Study ^b	Time to min ^c	Time to max ^c	Min % change	Max % change
1	3.4	10.3	-0.17	0.9
2	4.0	9.0	-0.40	1.5
3	2.4	6.4	-0.33	1.7
4	2.3	8.1	-0.26	1.0
Mean	3.0 ± 0.8	8.5 ± 1.6	-0.29 ± 0.10	1.3 ± 0.4

^aData obtained from the CC maps with the minimum CC coefficient of ~ 0.3 , demonstrating that the early dip was observed across the entire the area 18 of the cat primary visual cortex. The CNR for the positive BOLD was 16 ± 5 (ranging from 11 to 18) at 4.7 T and ~ 10 for 9.4 T.

^bAt 4.7 T, study #1–5 were obtained from Cat #1, study #6–7 from Cat #2, and study #8 from Cat #3. At 9.4 T, study #1–2 were obtained from the same cat while study #3 and #4 were obtained from two different cats.

^cTime to min. or max. are the time (in sec) it took to reach the minimum or maximum.

Table 2
Cross-Laboratory Comparison of the Early-Negative BOLD Responses^a

Species	Time to min (sec)	Min % change	TE (field)	Reference
Anesthetized cat	2.7 (2.9) ^b	-0.60 (-0.35) ^b	31 ms (4.7 T)	This study
	2.8 (3.0) ^b	-0.55 (-0.29) ^b	12 ms (9.4 T)	This study
	2.0-2.5	—	optical imaging	(9, 24)
Awake human	2.0	-1.0	30 ms (4.0 T)	(15, 16, 19)
	1.2	-0.4	60 ms (1.5 T)	(18)
	1-2	-0.5 ~ -1.0	20 ms (2.0 T)	(17)
Anesthetized monkey	2.5	-1.0	20 ms (4.7 T)	(20)

^aThe stimulus duration employed in all studies summarized here was ≥ 2 sec. It has been shown that the magnitude and the time-to-minimum of the early dip are essentially independent of stimulus duration for duration longer than ~ 3 sec in human (16). The magnitude and the time-to-maximum of the positive BOLD response, on the other hand, vary depending on the stimulus duration.

^bTwo values for the time-to-minimum as well as minimum percent-change are presented. One was obtained from the CC method (i.e., from Table 1) and the other was obtained from pixels that showed an early response between 0 and 4 sec (the entire dip) after stimulus onset. The former is showed in parentheses.

negative segments. Regions responding to the 45° stimulus appeared to be interdigitized and interleaved with those responding to the 135° stimulus—that is, the 45° and 135° “columns” appeared to cover complementary cortical spaces. The overlapped pixels (yellow) between the two stimuli were also observed. This is expected since the functional maps of these two orthogonal stimuli form only a subset of possible orientations, and the tuning curves for the orientation columns are broad (32). Note that these orthogonal functional maps were obtained using a *single* stimulus for each condition; no differential subtraction of one stimulus from its orthogonal counterpart was employed. Figure 4c,d showed the BOLD time courses obtained from the 45° stimulus (red time course, obtained from red + yellow pixels) and the 135° stimulus (green time course, obtained from green + yellow pixels). MR signals of the pixels representing the 45° “columns” show a large negative BOLD response *during the 45° stimulus* (red trace of Fig. 4c), but little or no negative response during the 135° stimulus (red trace of Fig. 4d). Similarly, those pixels representing the 135° “columns” (green trace of Fig. 4d) showed a large negative BOLD response *during*

the 135° stimulus, but little or no negative response during the 45° stimulus (green trace of Fig. 4c). Taken together, the interdigitized columnar maps of two orthogonal orientations and their temporal BOLD responses as well as the columnar size and spacing strongly indicate that columnar layouts were resolved based on the early-negative response without using the differential subtraction method.

Similarly, combined maps of two orthogonal orientations were generated using the early-positive segments (Fig. 5a,b). In marked contrast to the combined maps of the early-negative segments, the combined maps of the early-positive segments are clearly neither interleaved nor complementary. Rather, areas responding to similar orientations are grouped together into large regions with poor interdigitization. For example, in contrast to Fig 4b, the expanded view of Fig. 5b shows large clusters of red pixels with poor interdigitization with the green pixels. Figure 5c,d shows the BOLD time courses obtained from the 45° stimulus (red time course, obtained from red + yellow pixels) and the 135° stimulus (green time course, obtained from green + yellow pixels). The red traces show larger positive magnitudes at the plateau than the green trace

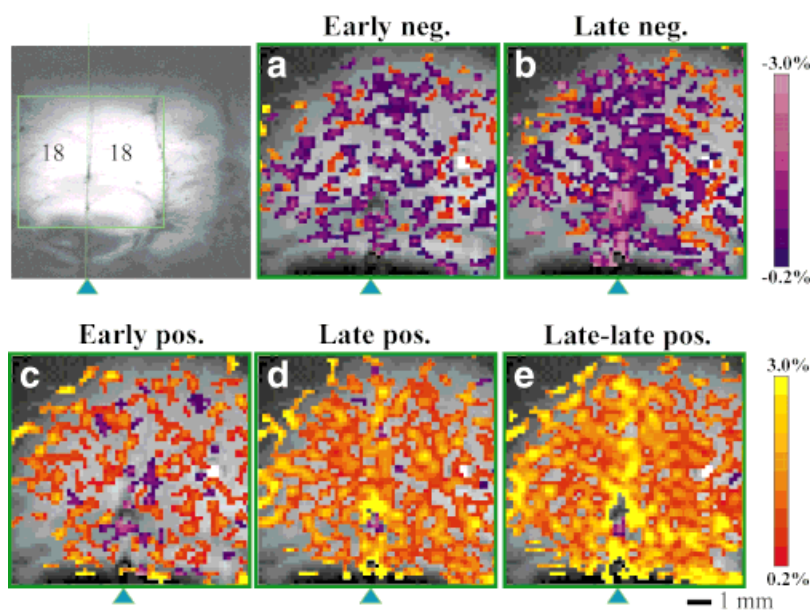
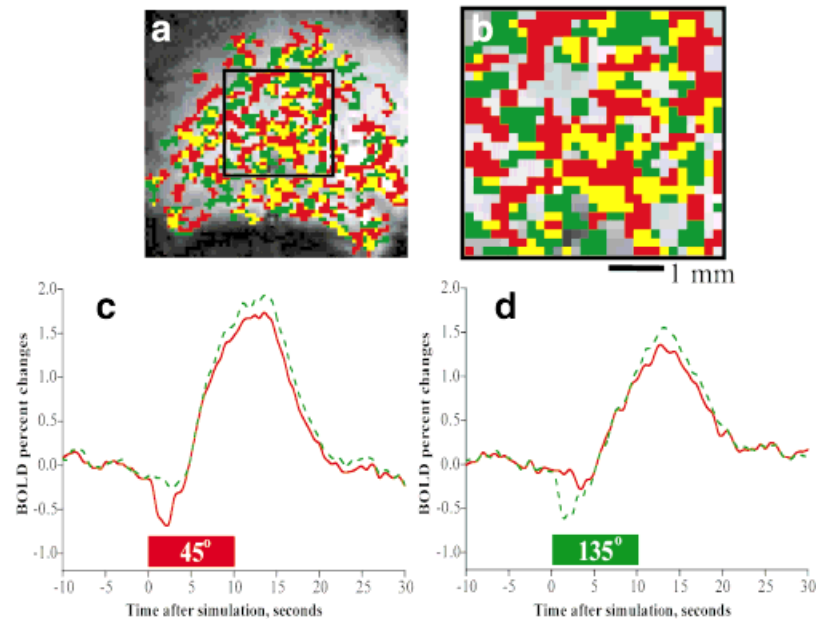


FIG. 3. Representative 2-sec time-binned, percent-change maps following a single orientation stimulus. A high-resolution anatomical (FLASH) image, tangential to the cortical surface shows the region of expansion of area 18 of the cat primary visual cortex. The dotted vertical line indicates the midline of the brain. **a**: “Time-binned” activation maps were obtained from the early-negative segment (0.5–2.0 sec after stimulus onset). **b**: Late-negative segment (2.5–4.0 sec). **c**: Early-positive segment (4.5–6.0 sec). **d**: Late-positive segment (6.5–8.0 sec). **e**: Late-late-positive segment (8.5–10 sec). Arrowheads indicate the position of the midline. The blue/purple and red/yellow colored bars indicate the negative and positive percent changes, respectively.

Early-negative maps of $45^\circ + 135^\circ$

FIG. 4. Combined activation maps of two orthogonal orientations using the early-negative segment. Activation maps from the 45° and 135° stimuli (a) and an expanded view (b) are shown in red and green, respectively. The common, overlapped pixels are shown yellow. Regions responding to the 45° stimulus appear to be highly interdigitized and spatially complementary with those responding to the 135° stimulus. c: BOLD time courses obtained from the 45° stimulus. The red (solid) time course was obtained from 45° columns (red + yellow pixels) during the 45° stimulus. The green (dashed) time course was obtained from the 135° columns (green + yellow pixels) during the 45° stimulus. d: Similar to c, except the stimulus was 135° . The green (dashed) time course was obtained from 135° columns (green + yellow pixels) during the 135° stimulus. The red (dashed) time course was obtained from the 45° columns (red + yellow pixels) during the 135° stimulus.



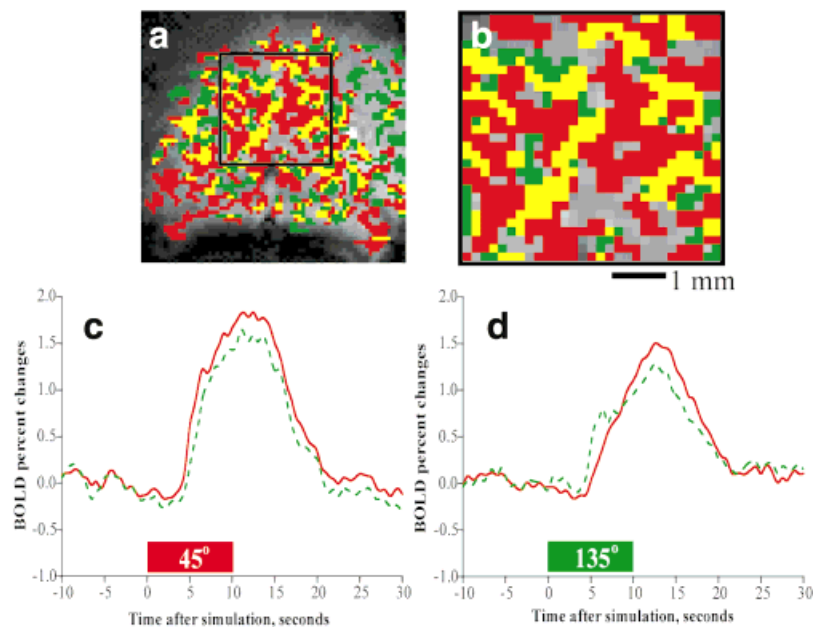
during both 45° and 135° stimulus. In other words, functional signal contrast reflecting the orthogonality of the stimulation condition was not readily discernable. In short, the early-positive response could not be readily used to resolve columnar layouts without using the differential subtraction method.

The test of complementary criterion was also applied to the late-positive BOLD responses of two *orthogonal* stimuli. Figure 6 shows the late-positive percent-change maps of 45° (a) and 135° (b) stimuli and their spatial overlaps. Pixels in and around large blood vessels (i.e., the superior

sagittal sinus) were discarded by disregarding pixels with large percent changes ($>2.1\%$) to avoid potential bias due to the large BOLD contrast around large vessels. Note that the same conclusions were reached without discarding these pixels. When the activation maps of two orthogonal stimuli were overlaid on top of each other, most pixels are common (yellow) pixels (Fig. 6c). The two orthogonal stimuli are clearly not complementary, even with a high threshold (Fig. 6d) and elimination of the large-vessel contribution. Similar analysis was also done for the CC maps (data not shown) and the same conclusions were reached.

Early-positive maps of $45^\circ + 135^\circ$

FIG. 5. Combined activation maps of two orthogonal orientations using the early-positive segment. Identical to Fig. 4 except the maps and time courses were generated using the early-positive segment instead of the early-negative segment. In marked contrast to the combined maps of the early-negative segment, the combined maps here are clearly not complementary. The corresponding time courses also show poor functional contrast for distinguishing “columns” responding the two orthogonal orientations.



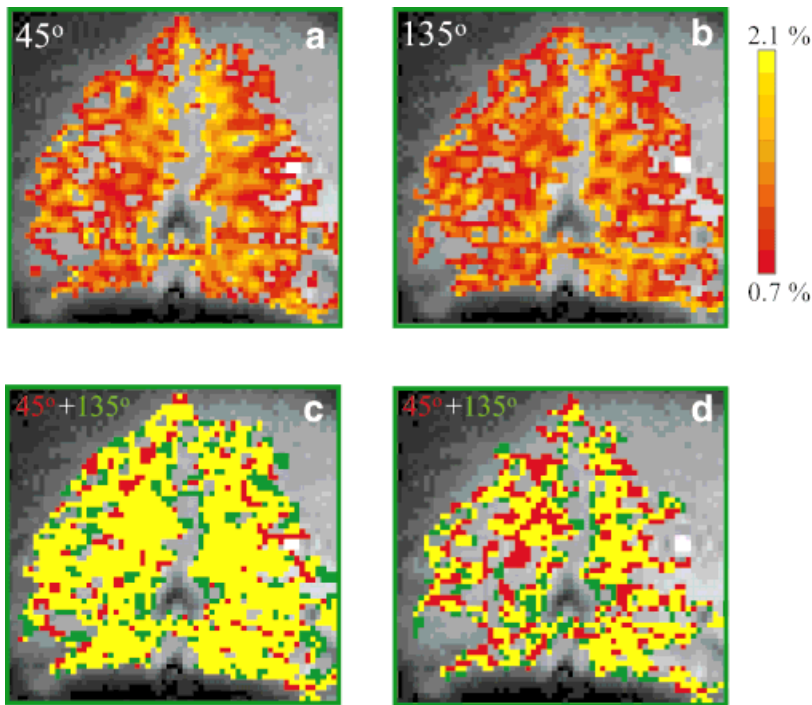


FIG. 6. Percent-change activation maps of two orthogonal orientations generated using the delayed positive BOLD response. Pixels in and around large blood vessels (i.e., the sagittal sinus) were discarded by cutting off pixels with large percent changes (2.1%) (a,b). Activation maps of the two orthogonal orientations (45° and 135°) were overlaid with the overlapped pixels shown in yellow (c,d). The two orthogonal stimuli are clearly not complementary at low (c) and high (d) statistical thresholds (0.7% and 1.0% changes, respectively).

These data clearly indicate that the delayed positive BOLD response is unsuitable for resolving columnar layouts under at least a single-stimulus condition without using the differential subtraction method.

Comparison of the Early-Negative and the Early-Positive Responses

Although the early-positive BOLD response was less suited for resolving columnar structures, it may yield important additional information to the early-negative response. We thus compared the activation maps generated using the early-negative and early-positive responses. Figure 7 shows a representative activation map generated by overlapping the early-negative segment (Fig. 3a) and the early-positive segment (Fig. 3c). The overlapped pixels are shown in yellow. The spatial registration of the early-negative and early-positive segment was significantly different, indicating that these two maps yielded different insight into the metabolic and hemodynamic responses associated with increased neuronal activity. The overlapping pixels constituted $22 \pm 6\%$ of the total active (colored) pixels.

Figure 7 also shows the corresponding BOLD time-courses of the activation maps generated with the early-negative (green, solid line) and early-positive segment (red, dashed line). The common pixels (yellow) between the two maps were excluded when generating these time-courses. The early-negative response curve shows a larger negative percent changes of -0.5% (average values: $-0.77 \pm 0.43\%$ at 4.7 T and $-0.94 \pm 0.20\%$ at 9.4 T) while the early-positive response curve showed little or no negative percent changes (average of $<-0.08\%$ for both fields). On the other hand, the early-negative response curve shows a smaller positive percent change of $\sim 1.0\%$ (average values: $1.07 \pm 0.37\%$ at 4.7 T and $1.00 \pm 0.33\%$ at 9.4

T) relative to the early-positive response curve of $\sim 1.5\%$ (average of $1.41 \pm 0.32\%$ at 4.7T and $1.34 \pm 0.44\%$ at 9.4T). The onset time toward positive magnitude of the early-negative response curve (~ 4 sec at both fields) is consistently and significantly longer than that of the early-positive response curve (~ 3 sec at both fields).

DISCUSSION

The results presented herein demonstrate that high spatio-temporal resolution BOLD studies of the cat visual cortex could be readily achieved by using EPI at 4.7 T and 9.4 T.

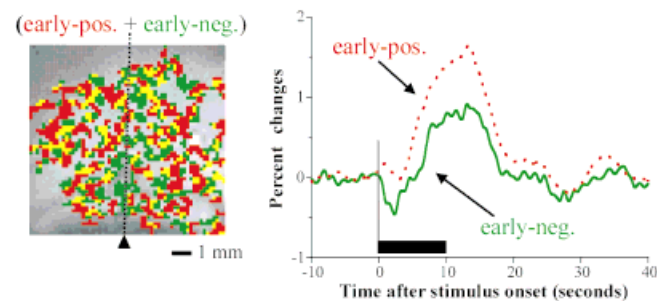


FIG. 7. (Left) A representative spatial “overlap” map between the early-negative and the early-positive segment and their corresponding time courses. The early-negative segment (purple/blue pixels of Fig. 3a) is shown in green and the early-positive segment (red/yellow pixels of Fig. 3c) is shown in red. The common pixels are shown in yellow. The spatial registration of the early-negative and early-positive segment was significantly different. The arrowhead indicates the position of the midline. (Right) Expanded time courses for the pixels that exhibit early-negative (green pixels, solid line) and early-positive response (red pixels, dashed line). The common pixels between the two maps were not included in the time courses.

This was made possible by the combination of hardware stability, animal physiology stability, small surface coil, and the time-efficient, high-contrast EPI technique. A transient early-negative BOLD response in area 18 of the cat primary visual cortex was consistently observed in essentially all BOLD fMRI measurements. The early-negative response peaked at ~ 3.0 sec following the stimulus onset, in excellent agreement with the optical imaging data (2.0–2.5 sec) obtained by using the identical animal model and stimulation paradigm, albeit different anesthetics (9,24). The negative-to-positive ratio of the BOLD percent change was ~ 0.22 , consistent with the negative-to-positive ratio (~ 0.33) of the deoxyhemoglobin signal reported in the optical imaging study (9). Since the BOLD contrast predominantly arises from the regional changes in deoxyhemoglobin, these consistencies with optical imaging data strongly indicate that the signal source of the BOLD response is identical to that of the optical deoxyhemoglobin signal. With the use of oxygen-sensitive phosphorescence dye, Vanzetta and Grinvald (25) recently demonstrated that the transient increase of intrinsic optical signal does indeed arise from a decrease in vascular oxygen tension. Therefore, the early-negative BOLD response is likely to reflect the initial metabolic $CMRO_2$ increase associated with functional stimulation before the cerebral blood flow (CBF) increase overcompensates for the needed metabolic demand.

It should, however, be noted that signal decreases in BOLD contrast could, in principle, also arise from an increase in cerebral blood volume (CBV) (5,33). An explanation of the early dip in terms of this mechanism was suggested by the “balloon” model (34). According to this model, the stimulus-induced CBF increase passively increases the CBV on the venous side. To date, there are no experimental data *directly* supporting or disproving this hypothesis. Indirect evidence from our laboratory (35,36), however, showed that the hypercapnia-induced CBV increase was found to be predominantly on the arteriole side, which does not give rise to significant BOLD contrast since the arterial side of the circulation does not contain significant deoxyhemoglobin (5,6). The hypercapnia-induced venous CBV increase, which is predominantly responsible for the BOLD contrast, was small (36). Thus, the delayed passive CBV increase downstream is unlikely to contribute significantly to the early-negative BOLD response. Interestingly, an active CBV increase resulting from capillary dilation immediately following increased neural activity has been suggested (24). This active CBV increase is likely to be more spatially specific compared to the passive CBV change. In any event, the CBV contribution to the early-negative BOLD response remains to be evaluated.

Although our cat data on the early dip are in general agreement with the human dip data, there were some major differences that are worth mentioning. The early-negative BOLD response in our dip data is more robust than that in human dip data. The early dip was observed without the use of a cross-correlation model to specifically pick out pixels exhibiting the early-negative response; in fact, the early dip was observed with an ROI containing essentially the entire area 18 of the cat visual cortex for the given imaging slice. This is in contrast to the human dip

data of Menon et al. (15), Hu et al. (16), and Yacoub et al. (18,19), who reported that the early dip was completely averaged out if all pixels that showed a positive response were considered. Second, the poststimulus undershoot was not consistently observed in our study. On the other hand, the poststimulus undershoot was quite consistently observed in human BOLD fMRI. The discrepancy between the human data and our cat data could be due to the difference in the relative stimulus strength. For example, the relatively mild drifting-grating stimulus used in our cat study compared to the relatively strong flashing-light stimulus (with darkness as the baseline) used in human may evoke a weaker neuronal, and thus a lower BOLD response. This notion is consistent with the relatively small positive percent change observed in our study in comparison to other BOLD studies in human. Other factors, including differences in stimulus duration and species, could contribute to this discrepancy. Third, the onset time of positive BOLD response in the anesthetized cats was about 4 sec, which is longer than the 2–3 sec onset time observed in awake humans. This difference could be due to the effect of anesthesia, which could result in a delay in the stimulus-induced CBF increase.

Interestingly, a previous BOLD study at 4.7 T in the cat visual cortex using the same stimulation paradigm and under essentially identical conditions as reported herein failed to detect the early dip (21). This discrepancy between Jezzard et al.’s (21) and our results may be due to differences in experimental parameters, CNR, SNR, instrument stability, physiological stability, and/or animal age. Notably, a FLASH imaging sequence was used in contrast to the EPI sequence used in our study. EPI is known to be much less sensitive to signal fluctuations induced by physiological processes (such as respiration-induced motion) and yields a higher sensitivity to the BOLD contrast. The temporal resolution was also coarser in their study and may have been inadequate to sample the early-negative response.

Similarly, BOLD fMRI studies of the forepaw stimulation in rat under α -chloralose anesthesia from this (22) and other (23) laboratories did not detect an early dip response. Instruments and methods used in our rat study were the same as in the cat study reported here and, thus, can be excluded as a cause of this discrepancy. Differences in functional task, anesthesia, and/or species may be responsible for the difference. In particular, the negative BOLD response may be more readily detectable in the visual cortex than in other cortical areas. It is also possible that different anesthetics may delay the CBF increase to a different extent, which modulated the initial deoxyhemoglobin accumulation. These and other hypotheses regarding the nature of the negative response remain to be vigorously tested.

Field-Dependence Comparison

Due to the significant difference in the measurement parameters used in this study, quantitative and direct comparisons of the BOLD responses at the two magnetic field strengths are not possible. For example, a single-shot EPI sequence was used at 4.7 T, whereas a two-shot EPI sequence was used at 9.4 T. Since the tissue T_2^* values at the

magnetic fields are different, a quantitative measure of the T_2^* changes associated with neural stimulation should yield a more robust field-dependence comparison. Nevertheless, despite these differences in parameters the ratio of the negative to positive BOLD response can be qualitatively compared based on the available data. The ratios of the negative to positive BOLD response at 4.7 T and 9.4 T were very similar, suggesting that the signal sources (and thus the spatial specificity) of the BOLD response are similar at both magnetic fields. Interestingly, in a recent study by Yacoub et al. (19), in which only the pixels exhibiting a negative response were considered (different from our analysis), the ratios of the negative-to-positive BOLD response were found to increase with increasing field strengths (~ 0.12 at 1.5 T, ~ 0.32 at 4.0 T). This is consistent with the notion that improved spatial specificity could be obtained at higher field (5,6). Differences in method of analysis and species prevent direct comparison between Yacoub et al. (19) and our study.

Spatiotemporal Dynamics and Specificity of the BOLD Response

Based on the “time-binned” percent-change maps, it could be demonstrated that the early-negative BOLD response (of the first 2 sec after stimulus onset) was spatially more confined than the late-late-positive or the conventional BOLD response. First, the activated pixels of the early-negative response were predominantly not in or around large vessels, while those of the late-late-positive BOLD response showed the highest level of activity in and around large vessels. Second, the number of activated pixels of the early-negative response was significantly less than that of the late-late-positive BOLD response after adjusting the statistical threshold for the CNR differences, suggesting that the former is less diffused than the latter. Finally, in marked contrast to the late-late-positive response the activation maps of the early-negative response appeared column-like and the maps of orthogonal orientations appeared complementary.

The regional deoxyhemoglobin signal as detected by the first 2 sec poststimulus onset appeared to drain from capillaries toward venules and into sinus, indicating that the entire dip did not necessarily yield high spatial specificity. In fact, the spatial specificity of the late-negative response was quite poor, similar to that of the late-late-positive response. Therefore, only the first ~ 2 sec of the early-negative response following the stimulus onset showed high spatial specificity that approximated columnar resolution. This conclusion is in marked contrast to previous studies (14–19), that generally stated that the entire dip is highly spatially localized.

Both the early-negative and the early-positive responses appeared to be well localized in comparison to the delayed positive BOLD response. However, only the columnar layouts obtained using the early-negative response were genuine based on the complementary criterion of orthogonal orientation stimuli and their corresponding BOLD time courses. Although the early-positive maps appeared patchy, their orthogonal orientation maps were not complementary. In some cases, complementary layouts from the early-positive BOLD responses of the two orthogonal

stimuli were observed by using the differential subtraction method. However, composite-angle (“pinwheel”) maps using four orientation stimuli did not exhibit the well-known characteristics of the orientation columns, as shown in our companion article (26). Based on these preliminary observations, the use of the differential subtraction method on the BOLD fMRI data should be used with caution, as it might not yield columnar layouts even though orthogonal maps might appear complementary. We further determined herein that the early-negative maps showed partial complementarity with the early-positive maps, suggesting that the activation map of the early-positive segment at least included “partial” inactive columns. This preliminary observation needs to be further investigated.

The entire BOLD signal dynamically evolves in the spatial domain as blood drains from active sites toward venules and large veins. The delayed positive response is most likely to be contaminated with large draining veins (which are reproducible but not functionally specific) unless measures are taken to eliminate the large-vessel contributions to the BOLD responses, i.e., by using high field, spin echo (37) and/or bipolar gradient (37,38). Therefore, to improve the spatial specificity of the BOLD response in general (whether or not an early-negative BOLD signal is observed) the first few seconds of the BOLD response should be used since they are likely to yield better spatial specificity relative to the later phase of the BOLD response.

Our data demonstrate that columnar layouts were not resolved using the late-positive BOLD responses, consistent with the optical imaging literature (9,24). This conclusion may appear to be inconsistent with that drawn by Yang et al. (39), who showed the conventional BOLD response could be used to localize activity to a single whisker barrel in the rat. This discrepancy between the whisker barrel and orientation column data, however, can be readily explained. Consider a hypothetical model of two different columnar spacings as shown in Fig. 8. The black rectangular box indicates the active column of $\sim 500 \mu\text{m}$. The CBF response is assumed to have a point-spread function (PSF) centered around the active structure. The BOLD response further depends on the CMRO₂ response in addition to the CBF PSF. In the whisker barrel study (39), only one whisker was selectively stimulated at a time and, thus, there was no overlap in the CBF PSF of neighboring active structures. This is analogous to Case I where the spacing between activated columns is large compared to the CBF PSF ($d \gg a$). Therefore, as long as the late BOLD and CBF responses showed the highest activity around the active sites, hemodynamic-based fMRI techniques can be readily used to localize a single column if neighboring columns were not activated at the same time. This conclusion still holds even if the hemodynamic response to the stimulus is diffused and/or become diffused with time.

On the other hand, orientation columns are generally not selectively stimulated one at a time but are stimulated in groups. The hemodynamic response of activated columns ($\sim 1.3 \text{ mm}$ apart) could potentially overlap, resulting in the failure to resolve individual active columns. Indeed, our data indicate this to be the case for the delayed positive BOLD response. Thus, the orientation column system is consistent with Case II in Fig. 8, where the distance between neighboring activated columns is on the order of

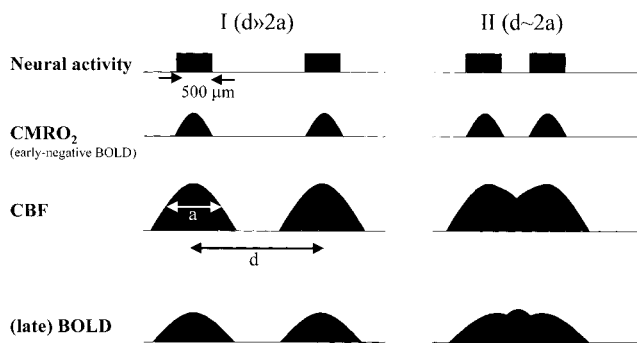


FIG. 8. Cartoons of the hypothetical CBF and BOLD responses for two different columnar spacings. The black rectangular box ideally symbolizes of the size of the active column ($\sim 500 \mu\text{m}$). The CMRO_2 increase, as reflected in the early-negative BOLD response, is highly spatially specific to the active column (based on 2-DG data). The distance between activated columns is characterized by “ d ” and the CBF PSF is characterized by “ a .” CBF response is assumed to have a point-spread function (PSF) around the active structure. The extent of the CBF PSF depends on the precise mechanism by which the task-induced CBF is upregulated and dissipated at the columnar level. The delayed BOLD response depends on the precise quantitative relationship among the intercolumnar spacings, the CBF PSF, and the CMRO_2 response. In Case I, the distance between columns responding to similar orientation stimulus is large compared to the CBF PSF ($d \gg a$). In Case II, the intercolumnar distance is on the order of the CBF PSF ($d \sim 2a$). Case II is consistent with the data on our cat orientation columns.

the CBF (and BOLD) PSF. The CBF responses in the active and inactive regions, and thus their ability to resolve individual active columns, depend on the quantitative relationship between the intercolumnar distance and the intrinsic hemodynamic response per se (CBF PSF). It is likely that active columns have a larger CBF changes than inactive columns and, thus, the use of the differential subtraction method or a high threshold could potentially be used to resolve individual columns. The BOLD responses further depend on the CMRO_2 response and the PSF of the BOLD susceptibility effect, in addition to the intrinsic hemodynamic PSF. It is possible that the larger BOLD response comes from the inactive columns. Interestingly, the use of the conventional BOLD response to map ocular dominance columns in human visual cortex has been attempted by using the differential subtraction method (13). The BOLD PSF and the intercolumnar distance were estimated to be $\sim 0.7 \text{ mm}$ and $\sim 1 \text{ mm}$, respectively (8). Based on the above discussions, there is a distinct possibility that the assignment of the left and right ocular dominance columns may be reversed. This remains to be validated by simultaneously measuring the BOLD and CBF response.

Finally, we would like to reiterate the potential challenges of using the early-negative BOLD signal for routine brain mapping at columnar resolution. Not only are good SNR and CNR as well as spatial and temporal resolutions necessary, but also the animal’s physiological stability is absolutely critical in eliciting a robust and consistent negative BOLD response. The early-negative BOLD technique developed herein is in principle applicable to mapping human functional columns. Its feasibility in practice, however, could potentially face considerable difficulty. Unlike

studies of anesthetized and mechanically ventilated animals, human studies pose the additional problem of head motion, which causes pixel misregistration. The magnitude of this dilemma is realized when one considers the dimensions of the pixels and the fact that both physiological variables (such as respiratory and heart beat) and conscious motion can easily cause image misalignment at columnar resolution. Further, since the entire BOLD signal is dynamically evolving in the temporal as well as the spatial domain as blood drains from the active sites toward the venules and large veins, a temporal threshold (i.e., the first 2 sec after the stimulus onset) must also be determined. Based on the aforementioned problems, mapping functional columns in the human brain using the early-negative BOLD signal is expected to be challenging.

CONCLUSIONS

Following the stimulus onset, a transient early-negative BOLD signal was observed in the cat primary visual cortex. The initially spatially localized early-negative BOLD signal appeared to dynamically drain from tissue areas into large veins. Only the early-negative response within 2 sec of the stimulus onset can achieve columnar resolution. By using the first 2 sec of the early-negative BOLD response, columns of $\sim 500 \mu\text{m}$ size separated by $\sim 1.3 \text{ mm}$ can be resolved. The MR-derived orientation columns obtained using two orthogonal stimuli are complementary. In a companion article (26), we further demonstrate that the MR-derived orientation columns are genuine by cross-validating with other quantitative key characteristics.

The delayed positive BOLD response appeared diffused and extended beyond tissue areas. The functional map generated using the delayed BOLD response thus has fundamental limitations in spatial resolution. Consequently, it is less suitable for mapping brain functions at columnar resolution if the distances between neighboring active columns are on the order of the BOLD PSF. The results presented herein have strong implications for the design and interpretation of BOLD fMRI experiments at the columnar level.

ACKNOWLEDGMENTS

The authors thank Mr. Essa Yacoub for stimulated discussions. S.G.K. is an Olmsted County Investigator (NAMI). A large part of this work was done during NIH postdoctoral support to T.Q.D. (NS10930).

REFERENCES

- Ogawa S, Lee T-M, Nayak AS, Glynn P. Oxygenation-sensitive contrast in magnetic resonance image of rodent brain at high magnetic fields. *Magn Reson Med* 1990;14:68–78.
- Ogawa S, Tank DW, Menon R, Ellermann JM, Kim S-G, Merkle H, Ugurbil K. Intrinsic signal changes accompanying sensory stimulation: functional brain mapping with magnetic resonance imaging. *Proc Natl Acad Sci USA* 1992;89:5951–5955.
- Kwong KK, Belliveau JW, Chesler DA, Goldberg IE, Weisskoff RM, Poncelet BP, Kennedy DN, Hoppel BE, Cohen MS, Turner R, Cheng H-M, Brady TJ, Rosen BR. Dynamic magnetic resonance imaging of human brain activity during primary sensory stimulation. *Proc Natl Acad Sci USA* 1992;89:5675–5679.

4. Bandettini PA, Wong EC, Hinks RS, Rikofsky RS, Hyde JS. Time course EPI of human brain function during task activation. *Magn Reson Med* 1992;25:390–397.
5. Ugurbil K, Hu X, Chen W, Zhu XH, Kim S-G, Georgopoulos A. Functional mapping in the human brain using high magnetic fields. *Philos Trans R Soc Lond B* 1999;354:1195–1213.
6. Ogawa S, Menon RS, Kim S-G, Ugurbil K. On the characteristics of functional magnetic resonance imaging of the brain. *Annu Rev Biophys Biomol Struct* 1998;27:447–474.
7. Engel A, Glover G, Wandell B. Retinotopic organization in human visual cortex and the spatial precision of functional MRI. *Cereb Cortex* 1997;7:181–192.
8. Menon RS, Goodyear BG. Submillimeter functional localization in human striate cortex using BOLD contrast at 4 Tesla: implications for the vascular point-spread function. *Magn Reson Med* 1999;41:230–235.
9. Malonek D, Grinvald A. Interactions between electrical activity and cortical microcirculation revealed by imaging spectroscopy: implications for functional brain mapping. *Science* 1996;272:551–554.
10. Turner R, Grinvald A. Direct visualization of patterns of deoxyhemoglobin and reoxygenation in monkey cortical vasculature during functional brain activation. In: *Proceedings of the SMRM 2nd Scientific Meeting, San Francisco, 1994*. p 430.
11. Lowel S, Freeman B, Singer W. Topographic organization of the orientation column system in large flat-mounts of the cat visual cortex: a 2-deoxyglucose study. *Exp Brain Res* 1988;71:33–46.
12. Shmuel A, Grinvald A. Functional organization for direction of motion and its relationship to orientation maps in cat area 18. *J Neurosci* 1996;16:6945–6964.
13. Menon RS, Ogawa S, Strupp JP, Ugurbil K. Ocular dominance in human V1 demonstrated by functional magnetic resonance imaging. *J Neurophysiol* 1997;77:2780–2787.
14. Ernst T, Hennig J. Observation of a fast response in functional MR. *Magn Reson Med* 1994;32:146–149.
15. Menon RS, Ogawa S, Hu X, Strupp JP, Anderson P, Ugurbil K. BOLD based functional MRI at 4 Tesla includes a capillary bed contribution: echo planar imaging correlates with previous optical imaging using intrinsic signals. *Magn Reson Med* 1995;33:453–459.
16. Hu X, Le TH, Ugurbil K. Evaluation of the early response in fMRI in individual subjects using short stimulus duration. *Magn Reson Med* 1997;37:877–884.
17. Janz C, Speck O, Hennig J. Time-resolved measurements of brain activation after a short visual stimulus: new results on the physiological mechanisms of the cortical response. *NMR Biomed* 1997;10:222–229.
18. Yacoub E, Hu X. Detection of the early negative response in fMRI at 1.5 Tesla. *Magn Reson Med* 1999;41:1088–1092.
19. Yacoub E, Le T, Ugurbil K, Hu X. Further evaluation of the initial negative response in functional magnetic resonance imaging. *Magn Reson Med* 1999;41:436–441.
20. Logothetis NK, Guggenberger H, Peled S, Pauls J. Functional imaging of the monkey brain. *Nat Neurosci* 1999;2:555–562.
21. Jezzard P, Rauschecker JP, Malonek D. An in vivo model for functional MRI in cat visual cortex. *Magn Reson Med* 1997;38:699–705.
22. Silva AC, Lee S-P, Iadecola C, Kim S-G. Early temporal characteristics of CBF and deoxyhemoglobin changes during somatosensory stimulation. *J Cereb Blood Flow Metab* 2000;20:201–206.
23. Marota JJA, Ayata C, Moskowitz MA, Weisskoff RM, Rosen BR, Mandeville JB. Investigation of the early response to rat forepaw stimulation. *Magn Reson Med* 1999;41:247–252.
24. Malonek D, Dirnagl U, Lindauer U, Yamada K, Kanno I, Grinvald A. Vascular imprints of neuronal activity: relationships between the dynamics of cortical blood flow, oxygenation, and volume changes following sensory stimulation. *Proc Natl Acad Sci USA* 1997;94:14826–14831.
25. Vanzetta I, Grinvald A. Cortical activity-dependent oxidative metabolism revealed by direct oxygen tension measurements; implications for functional brain imaging. *Science* 1999;286:1555–1558.
26. Kim D-S, Duong TQ, Kim S-G. High-resolution mapping of iso-orientation columns by fMRI. *Nat Neurosci* 2000;3:164–169.
27. Strupp JP. Stimulate: a GUI based fMRI analysis software package. *NeuroImage* 1996;3:S607.
28. Bandettini PA, Jesmanowicz A, Wong EC, Hyde JS. Processing strategies for time-course data sets in functional MRI of human brain. *Magn Reson Med* 1993;30:161–173.
29. Xiong J, Gao JH, Lancaster JL, Fox PT. Clustered pixels analysis for functional MRI activation studies of the human brain. *Human Brain Map* 1995;3:287–301.
30. Forman SD, Cohen JD, Fitzgerald M, Eddy WF, Mintun MA, Noll C. Improved assessment of significant activation in functional magnetic resonance imaging (fMRI): use of a cluster-size threshold. *Magn Reson Med* 1995;33:636–647.
31. Movshon JA, Thompson ID, Tolhurst DJ. Spatial and temporal contrast sensitivity of neurons in areas 17 and 18 of the cat's visual cortex. *J Physiol* 1978;283:101–120.
32. Bonhoeffer T, Grinvald A. Iso-orientation domains in cat visual cortex are arranged in pinwheel-like pattern. *Nature* 1991;353:429–432.
33. Ogawa S, Menon RS, Tank DW, Kim S-G, Merkle H, Ellermann JM, Ugurbil K. Functional brain mapping by blood oxygenation level-dependent contrast magnetic resonance imaging. *Biophys J* 1993;64:800–812.
34. Buxton RB, Wong EC, Frank LR. Dynamics of blood flow and oxygenation changes during brain activation: the balloon model. *Magn Reson Med* 1998;39:855–864.
35. Duong TQ, Kim S-G. In vivo MR measurements of regional arterial and venous blood volume fractions in intact rat brain. *Magn Reson Med* 2000;43:392–402.
36. Lee S-P, Duong TQ, Iadecola C, Kim S-G. Relationship between CBF and arterio-venous rCBV changes during hypercapnia in rat brain. In: *Proceedings of the 8th Annual Meeting of ISMRM, Denver, CO, 2000*. p 955.
37. Lee S-P, Silva AC, Ugurbil K, Kim S-G. Diffusion-weighted spin-echo fMRI at 9.4 T: microvascular/tissue contribution to BOLD signal change. *Magn Reson Med* 1999;42:919–928.
38. Boxerman JL, Bandettini PA, Kwong KK, Baker JR, Davis TL, Rosen BR, Weisskoff RM. The intravascular contribution to fMRI signal change: Monte Carlo modeling and diffusion-weighted studies in vivo. *Magn Reson Med* 1995;34:4–10.
39. Yang X, Hyder F, Shulman RG. Activation of single whisker barrel in rat brain localized by functional magnetic resonance imaging. *Proc Natl Acad Sci USA* 1996;93:475–478.
40. Lee J-H, Menon R, Andersen P, Truwit C, Garwood M, Ugurbil K. High contrast and fast three-dimensional magnetic resonance imaging at high fields. *Magn Reson Med* 1995;34:308–312.